

Conversion of phonon angular momentum into magnons in ferromagnets

Dapeng Yao* and Shuichi Murakami†
*Department of Physics, Tokyo Institute of Technology,
2-12-1 Ookayama, Meguro-ku, Tokyo 152-8551, Japan*
(Dated: July 28, 2023)

Chiral phonons carrying an angular momentum represent microscopic local rotations of atoms, which can be converted into electron spins so that the spin magnetizations are generated in crystals. In this paper, we find a new conversion of phonon angular momenta into magnons in a ferromagnet by using a spin-wave model with exchange and Dzyaloshinskii-Moriya interactions on a two-dimensional kagome lattice. We introduce valley-phonon modes with angular momenta, which modulate spin-spin interactions. The rotational motions are treated as an adiabatic process and it can dynamically affect the spin configuration due to geometric effects. We demonstrate that it is necessary to break both the inversion symmetry and spin-rotation symmetry along the quantization axis. Here, the inversion symmetry breaking results in the generation of a chiral phonon on a two-dimensional kagome lattice as has been proposed, and the spin-rotation symmetry breaking guarantees the non-trivial changes of the number of magnons due to chiral phonons. As a result, the clockwise and counterclockwise modes induce a change of the number of magnons with opposite signs, and the chiral nature of phonons can be reflected by the conversion of chiral phonons into magnons.

I. INTRODUCTION

Coupling between electron spins and rotational motions enables various conversion phenomena, such as the Einstein-de Haas [1] and the Barnett effect [2], in which the mechanical rotation of the crystal acts on the electron spin as an effective magnetic field [3–5]. Recently, chiral phonons, in which atomic motions have rotational modes, have been widely studied both in their theoretical formulations [6–12] and in experimental observations [13, 14]. In the valley-phonon modes with angular momenta, these atomic motions around their equilibrium positions hold a chiral nature.

In previous works, conversions of chiral phonon into the motions of electrons are studied theoretically by an adiabatic method. Because the masses of atoms are much larger than those of electrons, the motions of electrons adiabatically respond to the atomic rotations and these processes can be viewed as a slow chiral phonon. In this case, the contribution from chiral phonons can be treated by the Berry phase method [15, 16]. Under the setup of slow chiral phonons, one can show that chiral phonons in the honeycomb lattice generate a spin magnetization via spin-orbit coupling [17]. Moreover, in a chiral system with a helical crystal structure, in-plane chiral phonons induce a current along the helical axis, and the current induced by slow chiral phonons can have topological nature [18]. These previous studies shed light on the conversion of phonon angular momenta in paramagnetic electron systems.

On the other hand, spin waves, which are also dubbed as magnons, are collective propagations of precessional motions of magnetic moments [19, 20], and they govern many unconventional transport phenomena including

thermal Hall and spin Nernst effects [21–27] in magnetic systems. A spin-wave model on a pyrochlore lattice with Dzyaloshinskii-Moriya (DM) interaction has been proposed to investigate the magnon Hall effect in an insulating collinear ferromagnet $\text{Lu}_2\text{V}_2\text{O}_7$ [26]. Similar physics is seen in a spin-wave model on a two-dimensional (2D) kagome lattice [27], which corresponds to a (111) slice of the three-dimensional pyrochlore lattice. Accordingly, with the further understandings of chiral phonons, one can predict that the 2D kagome lattice can carry chiral phonons once the inversion symmetry is broken, in which clockwise (CW) and counterclockwise (CCW) rotational modes can appear at valley points connected by time reversal [9]. Therefore, the conversions between chiral phonons and magnons in ferromagnets become possible.

In this paper, we find a new phenomenon of a conversion of the phonon angular momentum into magnons in a ferromagnet with exchange and DM interactions. We find that chiral phonons modulate spin-spin interactions and induce time-dependent magnon excitations. The atomic rotations in chiral phonons are treated as slow and we show that they dynamically affect spin configurations. By means of the adiabatic approximation, chiral phonons can induce time-dependent magnon excitations, which has a non-zero time average of the change of the magnon number due to the geometric effect if the spin-rotation symmetry is broken. Intriguingly, the chiral phonons with CW and CCW modes induce a change in the number of magnons with opposite signs. Namely, they either increase or decrease the number of magnons due to the chiral nature of the atomic rotations. This new phenomenon predicted in this paper can be regarded as a ferromagnetic analogue of our previous paper [18], where we show that the chiral phonons induce electron spin polarizations in a paramagnet. Thus, we have shown that in addition to electron spins in a paramagnet [18], magnons in a ferromagnet are also induced by chiral phonons. In the case of magnons, we found that spin anisotropy plays

* yao.dapeng@stat.phys.titech.ac.jp

† murakami@stat.phys.titech.ac.jp

an essential role, and the proposed effect is universal in a wide range of ferromagnet.

The remainder of the paper is organized as follows. In Sec II, we introduce an anisotropic spin-wave Hamiltonian on the 2D kagome lattice with chiral phonons. Section III presents our theoretical treatments on magnon excitations induced by chiral phonons and discusses our results. Finally, we conclude our results in Sec IV. The details of our calculations on magnonic systems are placed in Appendix.

II. SPIN-WAVE MODEL WITH CHIRAL PHONONS

A. Anisotropic spin-wave Hamiltonian on 2D kagome lattice

We start from a quantum spin model with DM interaction on the 2D kagome lattice consisting of three sublattices A, B and C as shown in Fig. 1. Here, the z axis is set to be perpendicular to the 2D kagome-lattice plane, and $\mathbf{a}_1 = a(1/2, \sqrt{3}/2)$ and $\mathbf{a}_2 = a(-1/2, \sqrt{3}/2)$ are the primitive vectors of the lattice with the lattice constant a , and the vectors $\boldsymbol{\delta}_A = (0, 0)$, $\boldsymbol{\delta}_B = a(1/4, \sqrt{3}/4)$ and $\boldsymbol{\delta}_C = a(1/2, 0)$ label the relative positions of the sublattices A, B, and C with respect to the sublattice A. We notice that the bonds connecting adjacent sites form two types of triangles which are marked with red and blue in Fig. 1(b). The Hamiltonian is given by

$$H_0 = H_{\text{ex}} + H_{\text{DM}} + H_{\text{mag}}, \quad (1)$$

where the first term

$$H_{\text{ex}} = - \sum_{\langle i,j \rangle} (J_{ij}^x S_i^x S_j^x + J_{ij}^y S_i^y S_j^y + J_{ij}^z S_i^z S_j^z) \quad (2)$$

is the anisotropic XYZ spin model with different exchange parameters J_{ij}^x , J_{ij}^y and J_{ij}^z between electron spins located at the adjacent sites i and j . Here we suppose that the exchange parameters are different between the two types of the triangular unit cells. The exchange parameters are denoted by $J_{ij}^x = J_x$, $J_{ij}^y = J_y$, and $J_{ij}^z = J_z$ for the red triangle and $J_{ij}^x = J'_x$, $J_{ij}^y = J'_y$, and $J_{ij}^z = J'_z$ for the blue triangle. We set them to be different in order to break inversion symmetry, which is needed to have chiral phonons in the 2D kagome-lattice model [9]. If we set the exchange parameter to be isotropic $J_{ij}^x = J_{ij}^y = J_{ij}^z$, the first term H_{ex} reduces to an isotropic Heisenberg model.

The second term of the Hamiltonian in Eq. (1) is the DM interaction which is given by

$$H_{\text{DM}} = \sum_{\langle i,j \rangle} \mathbf{D}_{ij} \cdot (\mathbf{S}_i \times \mathbf{S}_j). \quad (3)$$

Here, \mathbf{D}_{ij} represents the DM interaction between the nearest-neighboring sites i and j , and $\mathbf{D}_{ij} = -\mathbf{D}_{ji}$. This

term is allowed since the midpoint between them is not a center of inversion. Since the directions of DM vectors are strongly constrained by the crystal symmetry, with the help of Moriya's rules [26–28], the DM vectors between each pair of nearest-neighboring sites can be obtained as

$$\mathbf{D}_{AC} = \mathbf{D}_{CB} = \mathbf{D}_{BA} = \frac{2D}{\sqrt{6}} \hat{\mathbf{e}}_z, \quad (4)$$

for the red triangles and

$$\mathbf{D}'_{AC} = \mathbf{D}'_{CB} = \mathbf{D}'_{BA} = \frac{2D'}{\sqrt{6}} \hat{\mathbf{e}}_z, \quad (5)$$

for the blue triangles. Here, these DM vectors have only the z component as shown in Fig. 1(b) with D and D' being the DM constants.

The third term of the Hamiltonian in Eq. (1)

$$H_{\text{mag}} = -g\mu_B \tilde{H} \sum_i S_i^z \quad (6)$$

represents the coupling with an external magnetic field $\tilde{H} = \tilde{H} \hat{\mathbf{e}}_z$ along the z axis, where g and μ_B denote the g factor of electrons and the Bohr's magneton, respectively. It is well known that in this spin model, the ground state is a collinear ferromagnet, and it is stable against the DM interaction. Here, since the component of the DM vector perpendicular to the direction of the external magnetic field does not contribute to the spin-wave Hamiltonian [26], only the z component of the DM vector D_{ij}^z should be retained in this model. Therefore, the second term Eq. (3) for the DM interaction can be expressed as $H_{\text{DM}} = \sum_{\langle i,j \rangle} D_{ij}^z (S_i^x S_j^y - S_i^y S_j^x)$.

Under the external magnetic field along the z axis, we take the z axis as a quantization axis of electron spins. To obtain the magnon spectrum, we introduce the ladder operators $S_i^\pm = S_i^x \pm iS_i^y$. Therefore, the anisotropic spin Hamiltonian is written as

$$H_0 = -\frac{1}{4} \sum_{\langle i,j \rangle} \left\{ 4J_{ij}^z S_i^z S_j^z + (J_{ij}^x - J_{ij}^y) (S_i^+ S_j^+ + S_i^- S_j^-) \right. \\ \left. + (J_{ij}^x + J_{ij}^y - i2D_{ij}^z) S_i^+ S_j^- + (J_{ij}^x + J_{ij}^y + i2D_{ij}^z) S_i^- S_j^+ \right\} \\ - g\mu_B \tilde{H} \sum_i S_i^z. \quad (7)$$

Then we apply the Holstein-Primakoff transformation

$$S_i^z = S - a_i^\dagger a_i, \\ S_i^+ = \left(2S - a_i^\dagger a_i \right)^{1/2} a_i \approx \sqrt{2S} \left(a_i - \frac{1}{4S} a_i^\dagger a_i a_i \right), \\ S_i^- = a_i^\dagger \left(2S - a_i^\dagger a_i \right)^{1/2} \approx \sqrt{2S} \left(a_i^\dagger - \frac{1}{4S} a_i^\dagger a_i^\dagger a_i \right), \quad (8)$$

where $a_i^\dagger(a_i)$ is the creation (annihilation) operator of magnons, and S represents the electron spin. When S is

large, the approximations in Eq. (8) become good. By using this transformation and neglecting the second terms in Eq. (8), the spin-wave Hamiltonian is finally expressed as

$$\begin{aligned}
H_0 = & -\frac{S}{2} \sum_{\langle i,j \rangle} (J_{ij}^x - J_{ij}^y) \left(a_i^\dagger a_j^\dagger + a_i a_j \right) \\
& -\frac{S}{2} \sum_{\langle i,j \rangle} J_{ij}^D \left(e^{i\phi_{ij}} a_i^\dagger a_j + e^{-i\phi_{ij}} a_j^\dagger a_i \right) \\
& + \sum_i (4J_z^D S + g\mu_B \tilde{H}) a_i^\dagger a_i, \quad (9)
\end{aligned}$$

where we introduce $J_{ij}^D = \sqrt{(J_{ij}^x + J_{ij}^y)^2 + 4(D_{ij}^z)^2}$ and $\phi_{ij} = \tan^{-1} \left(2D_{ij}^z / (J_{ij}^x + J_{ij}^y) \right)$, and the number 4 represents the number of the nearest-neighboring atoms. Thus, a quadratic form for the bosonic Hamiltonian has been finally obtained from the anisotropic spin-wave model.

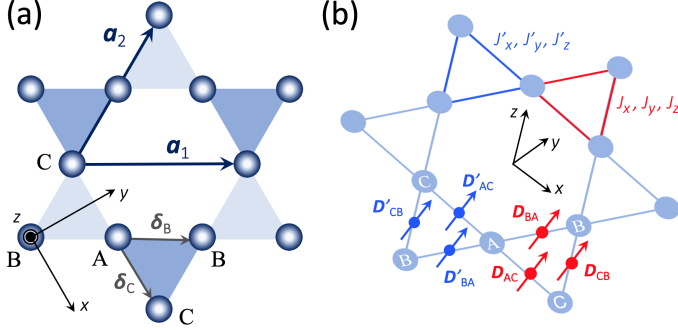


FIG. 1. (Color online). Two-dimensional kagome lattice. (a) Three sublattices A, B, and C are placed at each corner of the triangles with lattice vectors \mathbf{a}_1 and \mathbf{a}_2 . In each unit cell, the vectors δ_B and δ_C label the relative positions of the sublattice B and C to the sublattice A. (b) Dzyaloshinskii-Moriya vectors between two nearest-neighboring atoms are perpendicular to the xy plane and represented by red (blue) arrows at the midpoints of two sublattices. To break the inversion symmetry, DM vectors and exchange parameters are set to be different between the adjacent sites. The DM vectors and exchange parameters are marked as \mathbf{D}_{ij} , J_x , J_y , J_z in the red triangles and \mathbf{D}'_{ij} , J'_x , J'_y , J'_z in the blue triangles.

B. Magnon spectrum without chiral phonons

Here, we set $J_z = J'_z$ for simplicity, while the parameters J_x , J_y , and D for the red triangles and J'_x , J'_y , and D' for the blue triangles, are different. We also set $\lambda = \frac{D}{J_x + J_y} = \frac{D'}{J'_x + J'_y}$ for simplicity to guarantee that the angle ϕ_{ij} is common between the two types of triangles.

By means of the Fourier transformation

$$\begin{aligned}
a_{\mathbf{R}+\delta_m} &= \frac{1}{\sqrt{N}} \sum_{\mathbf{k}} e^{-i\mathbf{k}\cdot(\mathbf{R}+\delta_m)} a_{m,\mathbf{k}}, \\
a_{\mathbf{R}+\delta_m}^\dagger &= \frac{1}{\sqrt{N}} \sum_{\mathbf{k}} e^{i\mathbf{k}\cdot(\mathbf{R}+\delta_m)} a_{m,\mathbf{k}}^\dagger, \quad (10)
\end{aligned}$$

where $m = A, B$, and C denoting the three sublattices, N is the total particle numbers within the finite size of the crystal, \mathbf{R} represents the coordinate of the site, \mathbf{k} denotes the wave vector, and $a_{m,\mathbf{k}}^\dagger$ ($a_{m,\mathbf{k}}$) is the creation (annihilation) operator of the Bloch state with \mathbf{k} being the Bloch wavevector. Then, Eq. (9) becomes a bosonic Bogoliubov-de Gennes (BdG) Hamiltonian,

$$H_0 = \frac{1}{2} \sum_{\mathbf{k}} (\beta_{\mathbf{k}}^\dagger, \beta_{-\mathbf{k}}) \mathcal{H}_0(\mathbf{k}) \begin{pmatrix} \beta_{\mathbf{k}} \\ \beta_{-\mathbf{k}}^\dagger \end{pmatrix}, \quad (11)$$

where $\beta_{\mathbf{k}}^\dagger \equiv (a_{A,\mathbf{k}}^\dagger, a_{B,\mathbf{k}}^\dagger, a_{C,\mathbf{k}}^\dagger)$ represents the boson creation operators including the three internal degrees of freedom. The Bloch Hamiltonian of the spin-wave model in the momentum space reads

$$\mathcal{H}_0(\mathbf{k}) = \begin{pmatrix} \mathcal{A}_{0,\mathbf{k}} & \mathcal{A}_{1,\mathbf{k}} & \mathcal{A}_{2,\mathbf{k}} & 0 & \mathcal{B}_{1,\mathbf{k}} & \mathcal{B}_{2,\mathbf{k}} \\ \mathcal{A}_{1,\mathbf{k}}^* & \mathcal{A}_{0,\mathbf{k}} & \mathcal{A}_{3,\mathbf{k}} & \mathcal{B}_{1,\mathbf{k}}^* & 0 & \mathcal{B}_{3,\mathbf{k}} \\ \mathcal{A}_{2,\mathbf{k}}^* & \mathcal{A}_{3,\mathbf{k}}^* & \mathcal{A}_{0,\mathbf{k}} & \mathcal{B}_{2,\mathbf{k}}^* & \mathcal{B}_{3,\mathbf{k}}^* & 0 \\ 0 & \mathcal{B}_{1,-\mathbf{k}}^* & \mathcal{B}_{2,-\mathbf{k}}^* & \mathcal{A}_{0,-\mathbf{k}} & \mathcal{A}_{1,-\mathbf{k}}^* & \mathcal{A}_{2,-\mathbf{k}}^* \\ \mathcal{B}_{1,-\mathbf{k}} & 0 & \mathcal{B}_{3,-\mathbf{k}}^* & \mathcal{A}_{1,-\mathbf{k}} & \mathcal{A}_{0,-\mathbf{k}} & \mathcal{A}_{3,-\mathbf{k}}^* \\ \mathcal{B}_{2,-\mathbf{k}} & \mathcal{B}_{3,-\mathbf{k}} & 0 & \mathcal{A}_{2,-\mathbf{k}} & \mathcal{A}_{3,-\mathbf{k}} & \mathcal{A}_{0,-\mathbf{k}} \end{pmatrix}, \quad (12)$$

where

$$\begin{aligned}
\mathcal{A}_{0,\mathbf{k}} &= 4J_z S + g\mu_B \tilde{H}, \\
\mathcal{A}_{1,\mathbf{k}} &= -\frac{S}{2} e^{-i\phi} \{ J_D e^{-iK_{AB}} + J'_D e^{iK_{AB}} \}, \\
\mathcal{A}_{2,\mathbf{k}} &= -\frac{S}{2} e^{i\phi} \{ J_D e^{-iK_{AC}} + J'_D e^{iK_{AC}} \}, \\
\mathcal{A}_{3,\mathbf{k}} &= -\frac{S}{2} e^{-i\phi} \{ J_D e^{-iK_{BC}} + J'_D e^{iK_{BC}} \}, \\
\mathcal{B}_{1,\mathbf{k}} &= -S \{ (J_x - J_y) e^{-iK_{AB}} + (J'_x - J'_y) e^{iK_{AB}} \}, \\
\mathcal{B}_{2,\mathbf{k}} &= -S \{ (J_x - J_y) e^{-iK_{AC}} + (J'_x - J'_y) e^{iK_{AC}} \}, \\
\mathcal{B}_{3,\mathbf{k}} &= -S \{ (J_x - J_y) e^{-iK_{BC}} + (J'_x - J'_y) e^{iK_{BC}} \}, \quad (13)
\end{aligned}$$

with $J_D = \sqrt{(J_x + J_y)^2 + \frac{8D^2}{3}}$, $\phi = \tan^{-1} \left(\frac{4D}{\sqrt{6}(J_x + J_y)} \right)$, $K_{AB} = (k_x + \sqrt{3}k_y)a/4$, $K_{AC} = k_x a/2$, and $K_{BC} = (k_x - \sqrt{3}k_y)a/4$. Here $\mathcal{A}_{0,\mathbf{k}}$ denotes the on-site energy of magnons for which sublattices A, B, and C have no difference, and $\mathcal{A}_{1,\mathbf{k}}$, $\mathcal{A}_{2,\mathbf{k}}$, and $\mathcal{A}_{3,\mathbf{k}}$ ($\mathcal{B}_{1,\mathbf{k}}$, $\mathcal{B}_{2,\mathbf{k}}$, and $\mathcal{B}_{3,\mathbf{k}}$) represent the nearest neighbor interaction terms between the A-B, A-C, and B-C sublattices, respectively. We notice that both the exchange and the DM interaction contribute to $\mathcal{A}_{i,\mathbf{k}}$, and that $\mathcal{B}_{i,\mathbf{k}}$ ($i = 1, 2, 3$) has only the contributions from the x and y components of

the exchange interaction. The details of the diagonalization for the bosonic BdG Hamiltonian are given in Appendix A. The magnon bands can be obtained as shown in Fig. 2(b) with parameters $J_z = J'_z = 1$, $J_x = 0.8$, $J_y = 0.5$, $J'_x = 0.85$, $J'_y = 0.52$, $\lambda = 0.4$, and $S = 1/2$ without the external magnetic field ($\tilde{H} = 0$). Here the magnon dispersions are plotted along the high-symmetry points in Fig. 2(a). The bands above $E = 0$ are the magnon bands which are physically meaningful, and the bands below $E = 0$ are copies of the magnon bands because of the BdG form of the Hamiltonian, as discussed in Appendix A. The magnon spectrum is gapped, meaning that the ground state of this system is still ferromagnetic under the anisotropic exchange and the DM interaction. We notice that the bands at the \mathbf{K} and \mathbf{K}' point are not identical since we set that J_x , J_y , and D are different from J'_x , J'_y , and D' here, by which the inversion symmetry are broken.

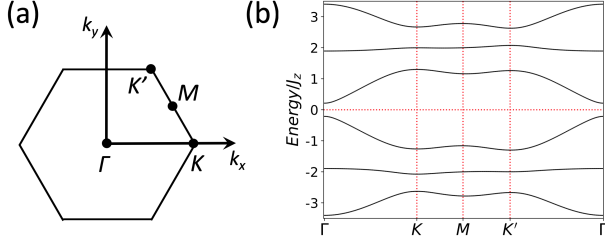


FIG. 2. (Color online). Magnon band structure of the spin-wave model. (a) The first Brillouin zone with the high-symmetry points for the kagome lattice in Fig. 1(a). (b) Magnon band structure from the spin-wave model with $J_z = J'_z = 1$, $J_x = 0.8$, $J_y = 0.5$, $J'_x = 0.85$, $J'_y = 0.52$, $\lambda = 0.4$, $S = 1/2$, and $\tilde{H} = 0$. There are three positive-definite bands above $E = 0$, and three bands below $E = 0$ are their copies.

C. Modulation of exchange parameters by chiral phonons

To find a model which can well describe ferromagnetic systems with chiral phonons, we add a perturbation term corresponding to chiral phonons into the static spin-wave Hamiltonian constructed in the previous subsection.

In general, the microscopic local rotation of atoms around their equilibrium positions carries a phase difference between adjacent atoms. In the present model, since the exchange parameters J_{ij}^a ($a = x, y, z$) and the DM vector D_{ij}^z are proportional to the overlap integrals between the atomic orbitals involved, they depend on the distance between the two adjacent magnetic atoms. In the presence of chiral phonons, the exchange parameters and the DM vectors should be modulated because the distance between two adjacent magnetic atoms changes periodically with time due to atomic rotations. Fig-

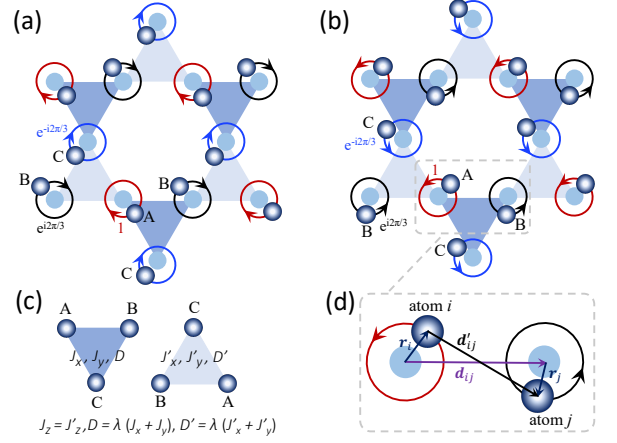


FIG. 3. (Color online). Two kinds of chiral phonon modes. Three atoms in each unit cell rotate in the xy plane with a certain phase correlation. The blue atoms rotate around their equilibrium positions with $\pm 2\pi/3$ phase difference. (a) Clockwise (CW) phonon mode at \mathbf{K} point. (b) Counterclockwise (CCW) phonon mode at \mathbf{K}' point. (c) Parameters of the upward triangles and the downward triangles are set to be different, which breaks inversion symmetry. (d) Two atoms i and j with their displacement vectors \mathbf{r}_i and \mathbf{r}_j from their equilibrium positions. Their relative positions are \mathbf{d}_{ij} and \mathbf{d}'_{ij} corresponding to the cases without and with rotational motion, respectively.

ure 3(d) shows the rotational motions of the two nearest-neighbor atoms i and j , where the displacement vectors relative to their equilibrium positions are set to be $\mathbf{r}_i(t)$ and $\mathbf{r}_j(t)$, which depend on the time t . It is reasonable to set the modulations of the spin-spin interactions to be proportional to the length change between the atoms given by $\mathbf{r}_{ij}(t) \cdot (\mathbf{d}_{ij}/a_0)$, where $\mathbf{r}_{ij}(t) = \mathbf{r}_j(t) - \mathbf{r}_i(t)$ and $a_0 = a/2$ for the kagome lattice. Thus, the exchange parameters and the DM vectors are modulated as $J_{ij}^\alpha \rightarrow J_{ij}^\alpha - \frac{J_{ij}^\alpha}{a_0} \mathbf{r}_{ij}(t) \cdot (\mathbf{d}_{ij}/a_0)$ ($\alpha = x, y, z$), and $D_{ij}^z \rightarrow D_{ij}^z - \frac{D_{ij}^z}{a_0} \mathbf{r}_{ij}(t) \cdot (\mathbf{d}_{ij}/a_0)$, respectively. Therefore, the parameter J_{ij}^D which couples the exchange parameter J_{ij}^x , J_{ij}^y , and the DM vector D_{ij}^z in the Eq. (9) should also be modulated as $J_{ij}^D \rightarrow J_{ij}^D - \frac{J_{ij}^D}{a_0} \mathbf{r}_{ij}(t) \cdot (\mathbf{d}_{ij}/a_0)$. Finally, the modulated spin-wave Hamiltonian with chiral phonons can be expressed as

$$\begin{aligned} \delta H(t) = & -\frac{S}{2} \sum_{\langle i,j \rangle} \frac{J_{ij}^x - J_{ij}^y}{a_0^2} \mathbf{r}_{ij}(t) \cdot \mathbf{d}_{ij} \left(a_i^\dagger a_j^\dagger + a_i a_j \right) \\ & -\frac{S}{2} \sum_{\langle i,j \rangle} \frac{J_{ij}^D}{a_0^2} \mathbf{r}_{ij}(t) \cdot \mathbf{d}_{ij} \left(e^{i\phi_{ij}} a_i^\dagger a_j + e^{-i\phi_{ij}} a_j^\dagger a_i \right) \\ & -\frac{S}{2} \sum_{\langle i,j \rangle} \frac{J_{ij}^z}{a_0^2} \mathbf{r}_{ij}(t) \cdot \mathbf{d}_{ij} \left(a_i^\dagger a_i + a_j^\dagger a_j \right), \end{aligned} \quad (14)$$

in which the last term can be cancelled if we set the parameter $J_z = J'_z$ as same as the one in the previous spin-wave model without chiral phonons. Therefore the modulated Hamiltonian $\delta H(t)$ has no diagonal terms with the chiral phonons here. Later we will use Eq. (14) with a certain phonon mode for the 2D kagome lattice.

D. Chiral phonons in 2D kagome lattice

The chiral phonons can emerge at the valley \mathbf{K} and \mathbf{K}' points if the inversion symmetry is broken by introducing the different spring constants between the two types of triangles (blue and red ones in Fig. 1(b)), and their vibration trajectories for the chiral phonons can be circular or elliptical in a 2D kagome lattice [9]. Here, as shown in Fig. 3(a) and (b), we consider two circular-polarized chiral-phonon modes, which appear at the \mathbf{K} point with a CW rotational mode and at the \mathbf{K}' point with a CCW rotational mode. In Fig. 3(a), the dis-

placement vectors of the sublattices A, B, and C for CW phonons are written as $\mathbf{r}_A^{\text{cw}} = r_0(\cos\omega t, -\sin\omega t)$, $\mathbf{r}_B^{\text{cw}} = r_0(\cos(\omega t - 2\pi/3), -\sin(\omega t - 2\pi/3))$, $\mathbf{r}_C^{\text{cw}} = r_0(\cos(\omega t + 2\pi/3), -\sin(\omega t + 2\pi/3))$, and Fig. 3(b) shows that the displacement vectors for CCW phonons are $\mathbf{r}_A^{\text{ccw}} = r_0(\cos\omega t, \sin\omega t)$, $\mathbf{r}_B^{\text{ccw}} = r_0(\cos(\omega t + 2\pi/3), \sin(\omega t + 2\pi/3))$, $\mathbf{r}_C^{\text{ccw}} = r_0(\cos(\omega t - 2\pi/3), \sin(\omega t - 2\pi/3))$ with the phonon frequency being ω . In this case, $\mathbf{r}_{ij}(t) \cdot \mathbf{d}_{ij}$ for the adjacent sublattices A-B, A-C, and B-C can be expressed as $\mathbf{r}_{AB}(t) \cdot \boldsymbol{\delta}_B = -\frac{\sqrt{3}ar_0}{2} \sin(\pm\omega t)$, $\mathbf{r}_{AC}(t) \cdot \boldsymbol{\delta}_C = -\frac{\sqrt{3}ar_0}{2} \sin(\pm\omega t + \pi/3)$, and $\mathbf{r}_{BC}(t) \cdot (\boldsymbol{\delta}_C - \boldsymbol{\delta}_B) = -\frac{\sqrt{3}ar_0}{2} \sin(\pm\omega t - \pi/3)$, where \pm represents the CW and CCW phonons, respectively.

By using the Fourier transformation Eq. (10), a Bloch Hamiltonian for the perturbation Eq. (14) can be written in a quadratic form of a bosonic operators as

$$\delta H(t) = \frac{1}{2} \sum_{\mathbf{k}} (\beta_{\mathbf{k}}^\dagger, \beta_{-\mathbf{k}}) \delta \mathcal{H}(\mathbf{k}, t) \begin{pmatrix} \beta_{\mathbf{k}} \\ \beta_{-\mathbf{k}}^\dagger \end{pmatrix}, \quad (15)$$

with

$$\delta \mathcal{H}(\mathbf{k}, t) = \begin{pmatrix} 0 & \delta \mathcal{A}_{1,\mathbf{k}} & \delta \mathcal{A}_{2,\mathbf{k}} & 0 & \delta \mathcal{B}_{1,\mathbf{k}} & \delta \mathcal{B}_{2,\mathbf{k}} \\ \delta \mathcal{A}_{1,\mathbf{k}}^* & 0 & \delta \mathcal{A}_{3,\mathbf{k}} & \delta \mathcal{B}_{1,\mathbf{k}}^* & 0 & \delta \mathcal{B}_{3,\mathbf{k}} \\ \delta \mathcal{A}_{2,\mathbf{k}}^* & \delta \mathcal{A}_{3,\mathbf{k}}^* & 0 & \delta \mathcal{B}_{2,\mathbf{k}}^* & \delta \mathcal{B}_{3,\mathbf{k}}^* & 0 \\ 0 & \delta b_{1,-\mathbf{k}}^* & \delta \mathcal{B}_{2,-\mathbf{k}} & 0 & \delta \mathcal{A}_{1,-\mathbf{k}}^* & \delta \mathcal{A}_{2,-\mathbf{k}}^* \\ \delta \mathcal{B}_{1,-\mathbf{k}} & 0 & \delta \mathcal{B}_{3,-\mathbf{k}}^* & \delta \mathcal{A}_{1,-\mathbf{k}} & 0 & \delta \mathcal{A}_{3,-\mathbf{k}}^* \\ \delta \mathcal{B}_{2,-\mathbf{k}} & \delta \mathcal{B}_{3,-\mathbf{k}} & 0 & \delta \mathcal{A}_{2,-\mathbf{k}} & \delta \mathcal{A}_{3,-\mathbf{k}} & 0 \end{pmatrix}. \quad (16)$$

Here the elements of the Bloch Hamiltonian for the perturbation are

$$\begin{aligned} \delta \mathcal{A}_{1,\mathbf{k}} &= -\frac{S}{2} e^{-i\phi} \{ \delta J_D e^{-iK_{AB}} + \delta J'_D e^{iK_{AB}} \} \sin(\pm\omega t), \\ \delta \mathcal{A}_{2,\mathbf{k}} &= -\frac{S}{2} e^{i\phi} \{ \delta J_D e^{-iK_{AC}} + \delta J'_D e^{iK_{AC}} \} \sin(\pm\omega t - \frac{\pi}{3}), \\ \delta \mathcal{A}_{3,\mathbf{k}} &= -\frac{S}{2} e^{-i\phi} \{ \delta J_D e^{-iK_{BC}} + \delta J'_D e^{iK_{BC}} \} \sin(\pm\omega t + \frac{\pi}{3}), \\ \delta \mathcal{B}_{1,\mathbf{k}} &= -\sqrt{3}S \{ C_b e^{-iK_{AB}} + C'_b e^{iK_{AB}} \} \sin(\pm\omega t), \\ \delta \mathcal{B}_{2,\mathbf{k}} &= -\sqrt{3}S \{ C_b e^{-iK_{AC}} + C'_b e^{iK_{AC}} \} \sin(\pm\omega t - \frac{\pi}{3}), \\ \delta \mathcal{B}_{3,\mathbf{k}} &= -\sqrt{3}S \{ C_b e^{-iK_{BC}} + C'_b e^{iK_{BC}} \} \sin(\pm\omega t + \frac{\pi}{3}), \end{aligned} \quad (17)$$

where $\delta J_D = r_0 \sqrt{(J_x + J_y)^2 + \frac{8D^2}{3}}/a_0$, $\delta J'_D = r_0 \sqrt{(J'_x + J'_y)^2 + \frac{8D'^2}{3}}/a_0$, $C_b = \delta J_x - \delta J_y$, $C'_b = \delta J'_x - \delta J'_y$ with $\delta J_\alpha = J_\alpha r_0/a_0$ ($\alpha = x, y$). Here r_0 denotes the amplitude of the atomic motions, and we set $r_0 = 0.1a_0$ in the following calculation as an example, which means the displacement is around 10% of the lattice constant [17, 18]. The details of our calculations will be shown later.

III. MAGNON EXCITATIONS INDUCED BY CHIRAL PHONONS

In our assumption of slow chiral phonons, the atomic rotations adiabatically affect the spin configurations of electrons so that the magnon dynamics is induced by chiral phonons. In this section, we investigate the change of the number of the magnons based on the modulated spin-wave model by means of Berry phase treatment on chiral phonons [16–18].

A. Geometric term arising from Berry phase treatment

The Berry phase treatment has already been applied to electron systems for calculating orbital magnetization, spin magnetization and current under adiabatic process [16–18]. It starts from a periodically time-dependent Hamiltonian H_t which changes slowly enough compared to the electronic energy scale. Let $|\psi_n(t)\rangle$ be an instantaneous eigenstate of the band n at time t . The expectation value of the operator \hat{X} that we are interested in under

the adiabatic process can be obtained as

$$X(t) = \sum_n^{\text{occ}} (X_n^{\text{inst}}(t) + X_n^{\text{geom}}(t)). \quad (18)$$

Here, the first term

$$X_n^{\text{inst}}(t) \equiv \hbar \langle \psi_n(t) | \hat{X}(t) | \psi_n(t) \rangle \quad (19)$$

is called an instantaneous term and the second term

$$X_n^{\text{geom}}(t) \equiv \sum_{m(\neq n)} \left\{ \frac{\hat{X}_{nm}(t) A_{mn}(t)}{E_n(t) - E_m(t)} + \text{c.c.} \right\} \quad (20)$$

is dubbed as a geometric term with the matrix elements $\hat{X}_{nm}(t) = \langle \psi_n(t) | \hat{X}(t) | \psi_m(t) \rangle$ of the operator $\hat{X}(t)$, and the Berry phase $A_{mn}(t) = \langle \psi_m(t) | (-i\partial_t) | \psi_n(t) \rangle$. The formulation of Eq. (18) is for fermionic systems and it is expressed as the sum \sum_n^{occ} over all the occupied states at the absolute zero temperature. In bosonic systems, one should replace Eq. (18) with a corresponding formula with the Bose distribution function.

B. Change of the number of magnons by chiral phonons

Since the chiral phonons on the 2D kagome lattice modulate the exchange parameters, the Bloch state of the time-dependent spin-wave Hamiltonian will change with time. The most straightforward way to study this is to calculate the number of the magnons. Between the two terms, the instantaneous term and the geometric term, only the geometric term can give a non-trivial result, which reflects the phonon chirality, because the geometric term represents path-dependent dynamics in terms of the Berry connection during the adiabatic process. The geometric terms of the CW and CCW phonons have the opposite paths in the phase space, which causes opposite changes of the number of magnons. On the other hand, the instantaneous term represents the snapshot at time t , and unlike the geometric term, the instantaneous term has no difference between the CW and CCW phonons.

Now, we consider the number operator of magnons \hat{N} as the operator \hat{X} . Then, we need to rewrite Eq. (18) to incorporate the Bose distribution function. To avoid the singularity of the Bose distribution function at zero temperature, we set the temperature to be nonzero and then Eq. (20) should be revised accordingly by incorporating the Bose distribution function as

$$N_n^{\text{geom}}(\tau) = \frac{\hbar\omega}{S_{xy}} \sum_{m(\neq n)} \sum_{\mathbf{k}} \left\{ \frac{\hat{N}_{nm}(\mathbf{k}, \tau) A_{mn}(\mathbf{k}, \tau)}{E_{n,\mathbf{k}}(\tau) - E_{m,\mathbf{k}}(\tau)} \right\} f_{n,\mathbf{k}}, \quad (21)$$

where

$$\hat{N}_{nm}(\mathbf{k}, \tau) = \langle \psi_{n,\mathbf{k}}(\tau) | \hat{N}(\tau) | \psi_{m,\mathbf{k}}(\tau) \rangle \quad (22)$$

is the off-diagonal matrix element of the number operator of magnons, and

$$\begin{aligned} A_{mn}(\mathbf{k}, \tau) &= \langle \psi_{m,\mathbf{k}}(\tau) | (-i\partial_\tau) | \psi_{n,\mathbf{k}}(\tau) \rangle \\ &= -i \frac{\langle \psi_{m,\mathbf{k}}(\tau) | \partial_\tau \mathcal{H}(\mathbf{k}, \tau) | \psi_{n,\mathbf{k}}(\tau) \rangle}{E_{n,\mathbf{k}}(\tau) - E_{m,\mathbf{k}}(\tau)} \end{aligned} \quad (23)$$

is the matrix element of the Berry connection. Here, we introduce a dimensionless quantity $\tau = \omega t$ to replace the time t , S_{xy} represents the size of the 2D unit cell within the xy plane, and $f_{n,\mathbf{k}} = f(E_{n,\mathbf{k}})$ is the Bose distribution function for the n -th band. $N_n^{\text{geom}}(\tau)$ as a function of τ becomes proportional to the phonon frequency ω because the Berry connection contains the time derivative terms. Finally, the expectation value of the total magnon number from the geometric terms becomes

$$N_{\text{tot}}^{\text{geom}}(\tau) = \sum_n N_n^{\text{geom}}(\tau). \quad (24)$$

The details of the calculation of the geometric term within the bosonic BdG formalism is discussed in Appendix B. We notice that the geometric term involves the off-diagonal elements of the number operator of magnons. If we consider an isotropic spin-wave model, however, the number operator of magnons can be simultaneously diagonalized with the isotropic spin-wave Hamiltonian because of the SU(2) spin-rotation symmetry. Therefore, the isotropy results in a zero geometric term of the number of magnons. That is why we introduce an anisotropic spin-wave model in this paper in order to obtain a nonzero change of the magnon excitations induced by chiral phonons.

Figure 4 shows the expectation value of the number of magnons from the geometric term as a function of the dimensionless time τ , and Fig. 4(a-1)-(a-4) and Fig. 4(b-1)-(b-4) are for the CW and CCW phonons, respectively. Here, N_1^{geom} , N_2^{geom} , and N_3^{geom} are the contributions from the first, the second, and the third bands, respectively, and $N_{\text{tot}}^{\text{geom}}$ is their sum. We set the temperature $k_B T = 2J_z$ for the Bose distribution function. The values of the middle numbers on the vertical axis showed in each figure represent their time average during a period of 2π for τ .

The results show that time averages of the number of magnons induced by the CW and CCW phonons have the same values but opposite signs for each band. The time-dependent Bloch Hamiltonians between the CW and CCW phonons can be connected by changing the sign of the dimensionless time τ : $\mathcal{H}^{\text{CW}}(\mathbf{k}, \tau) = \mathcal{H}^{\text{CCW}}(\mathbf{k}, -\tau)$, because the CW and CCW phonons have the opposite directions of rotational motions and are mutually related via the time-reversal $\tau \rightarrow -\tau$. Hence the matrix elements of the number operator of magnons satisfy $\hat{N}_{nm}^{\text{CW}}(\mathbf{k}, \tau) = \hat{N}_{nm}^{\text{CCW}}(\mathbf{k}, -\tau)$, and the matrix elements of the Berry connection: $A_{mn}^{\text{CW}}(\mathbf{k}, \tau) = -A_{mn}^{\text{CCW}}(\mathbf{k}, -\tau)$. Therefore, the geometric terms of the number of magnons of the CW and CCW phonons are related by $N_n^{\text{CW}}(\tau) = -N_n^{\text{CCW}}(-\tau)$ in agreement with the numerical results in Fig. 4(a-1)-(a-4) and Fig. 4(b-1)-(b-4).

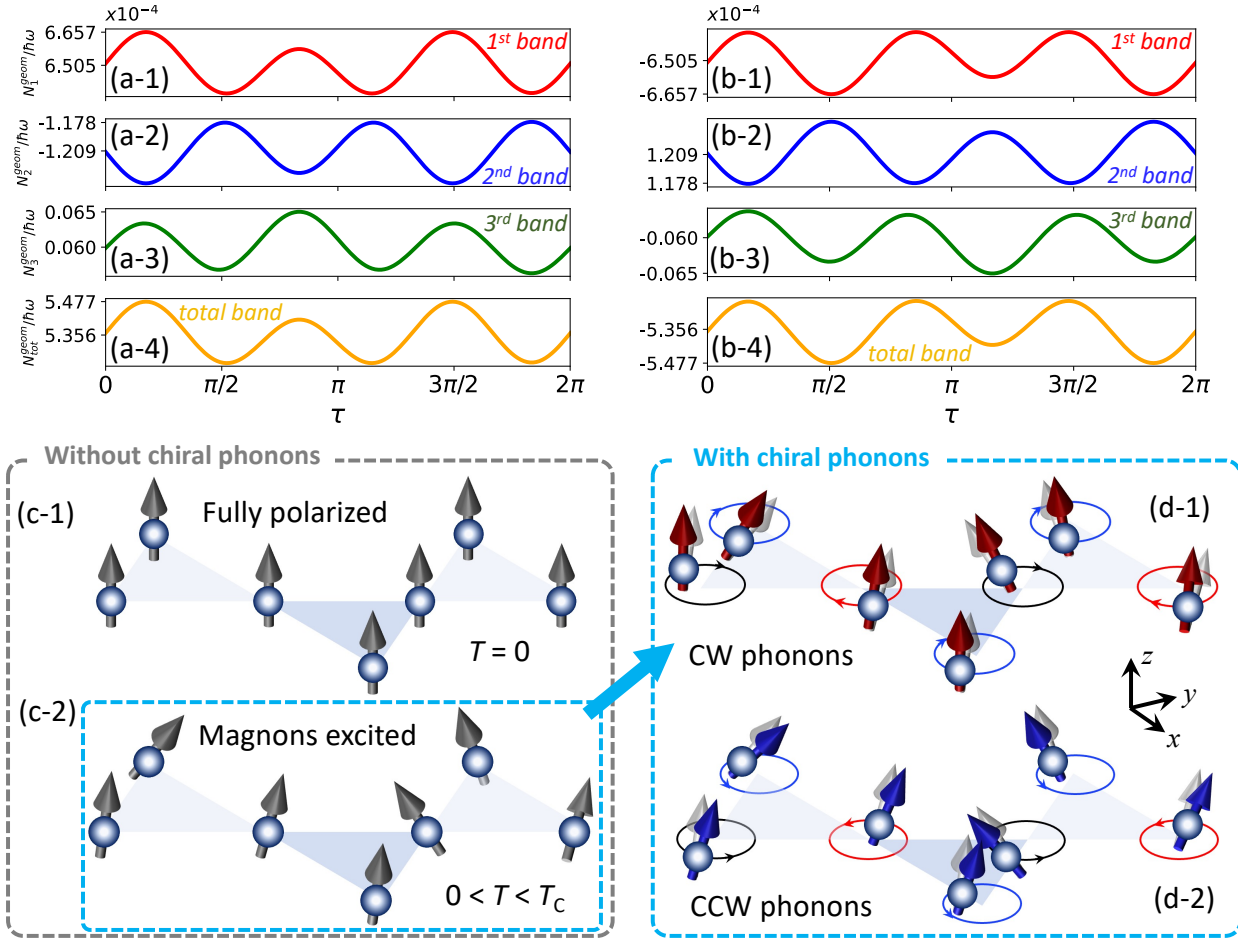


FIG. 4. (Color online). The number of magnons varying with the dimensionless time τ for one period. (a)(b) Magnon excitation by (a) CW phonons and (b) CCW phonons. Here red, blue, and green lines represent the number of magnons from the first, second, and third bands, and orange lines represent their sum. The middle number on the vertical axis represents the time average over one period $0 \leq \tau \leq 2\pi$. The parameters are set to be $J_z = J'_z = 1$, $J_x = 0.8$, $J_y = 0.5$, $J'_x = 0.85$, $J'_y = 0.52$, $r_0 = 0.1a_0$, $\lambda = 0.4$, $S = 1/2$, and $\vec{H} = 0$. (c-1) and (c-2) show schematic figures of spin configuration without chiral phonons at $T = 0$ (fully polarized) and at $0 < T < T_c$ (magnon excited), respectively. (d-1) and (d-2) show the changed spin configuration relative to (c-2) due to chiral phonons with CW and CCW modes, respectively.

In the absence of chiral phonons, spin magnetization are fully polarized at absolute zero temperature $T = 0$, in which magnons are not excited as shown in Fig. 4(c-1). Once the temperature becomes finite but below the transition temperature T_c , magnons are excited, and spin magnetizations decrease with a precessional motion shown in Fig. 4(c-2). Within our toy model, in the presence of the slow chiral phonons, the geometric effect gives a change of the number of magnons, and it corresponds to the time-dependent geometric term with a non-zero time average, which either increases or decreases the number of magnons. Figures 4(d-1) and (d-2) give a schematic picture of this process corresponding to our numerical calculations, in which the number of magnons increases with CW phonons and decreases with CCW phonons,

respectively. The opposite change of spin magnetization due to the chiral phonons with the opposite rotational modes reflects the chiral nature of the phonons. It shows a conversion of chiral phonons into magnons under an adiabatic process.

Changes of the number of magnons represents spin dynamics of electrons. $N_{\text{tot}}^{\text{geom}}(\tau)$ in Eq. (24) means the expectation value of the magnon number per unit area in the xy plane. Therefore, the magnon number per one localized spin is $N_{\text{tot}}^{\text{geom}} S_{\text{uc}}/3$ with the size of the unit cell $S_{\text{uc}} = \sqrt{3}a^2/2$ because the unit cell contains three spins. The numerical results in Fig. 4(a-4)(b-4) show that $N_{\text{tot}}^{\text{geom}}$ is about $10^{-4} \times \hbar\omega a^2$, which means that the total magnon number per localized spin is about 10^{-5} if we take $\hbar\omega = 0.1J_z = 0.1$ as an example. This value is to

be compared with the total spin $S = 1/2$ (see Eq. (8)). Thus, if we assume that the rotational radius of atoms around their equilibrium positions is about 10% of the lattice constant within our model calculation, the change of the spin polarization due to the geometrical effect by the chiral phonons is about 10^{-5} of the full polarization.

We comment that in reality the phonon amplitude is less than 10%, and the estimated magnitude of the effect will be smaller. On the other hand, within our theory because the effect is proportional to the phonon frequency (see Eq. (21)), the effect will be much enhanced when the phonon frequency becomes larger. In our paper we take an adiabatic approximation, which is valid when $\hbar\omega/J_z \ll 1$, and we take $\hbar\omega/J_z = 0.1$ in our calculation. Behaviors of this effect for larger values of the phonon frequency ω beyond the adiabatic approximation will be interesting and is left as a future work.

IV. CONCLUSION

In this paper, we have theoretically proposed a new conversion between chiral phonons and magnons in ferromagnets. We construct a spin-wave model with anisotropic exchange and DM interactions on a 2D kagome lattice to study the dynamics of magnon excitations due to chiral phonons. We need to break the inversion symmetry in order to generate chiral phonons on the 2D kagome lattice, and we also need to introduce anisotropy of the spin-spin interaction in our spin model to break spin-rotation symmetry with respect to the z direction. The resulting spin-wave Hamiltonian becomes of the BdG type. Our model is intended to be a minimal model to demonstrate a new type of magnon excitations induced by slow chiral phonons from the geometric effects.

By treating the atomic rotations as an adiabatic process, we find that the time-dependent number of magnons has two terms: the instantaneous term and the geometric term. The instantaneous term is trivially given by a snapshot at the given time, so the instantaneous term will be of no difference between the CW and CCW phonon modes. On the other hand, for the geometric term, intriguingly the time averages of the number of magnons induced by the CW and CCW phonons have the same values but opposite signs. Thus, the phonon chirality is reflected by the geometric effect here.

In the present paper, we studied the chiral phonon at the \mathbf{K} and \mathbf{K}' valleys with phonon angular momenta. In a 2D kagome lattice, the orbits for the chiral phonons can be circular or elliptical and they must have the same chirality [9]. Here, we only considered circular-polarized rotations, and we expect that even elliptical chiral phonons would give the same physics, whose calculation may be more complicated than that in the present setup. On the other hand, different from the previous studies related to phonon-magnon coupling [29, 30], in our method, the contribution from chiral phonons is ab-

sorbed as time-dependent parameters into the magnon Hamiltonian. Here, even though the coupling of chiral phonons and magnons is taken into account, we can still simply deal with it as a single-particle problem for magnons. Thus, the similar method can also be used to investigate general systems with slow chiral phonons. On the other hand, for phonons with higher frequency, the effect predicted in this paper will become larger but its calculation is beyond the scope of the Berry phase method we used in the present paper. Such behaviors of the chiral phonon with higher frequency are left as future problems.

ACKNOWLEDGMENTS

This work was partly supported by JSPS KAKENHI Grants No. JP20H04633, No. JP22H00108, and No. JP23KJ0926, and also by MEXT Initiative to Establish Next-generation Novel Integrated Circuits Centers (X-NICS) Grant No. JPJ011438.

Appendix A: Diagonalization of bosonic BdG Hamiltonian

In this appendix, we provide more details about the diagonalization of a generic bosonic BdG Hamiltonian [19, 20]. As we showed in the main text, the generic bosonic BdG Hamiltonian can be expressed as

$$H = \frac{1}{2} \sum_{\mathbf{k}} (\beta_{\mathbf{k}}^\dagger, \beta_{-\mathbf{k}}) \mathcal{H}(\mathbf{k}) \begin{pmatrix} \beta_{\mathbf{k}} \\ \beta_{-\mathbf{k}}^\dagger \end{pmatrix}, \quad (\text{A1})$$

with $\beta_{\mathbf{k}}^\dagger \equiv (a_{1,\mathbf{k}}^\dagger, a_{2,\mathbf{k}}^\dagger, \dots, a_{M,\mathbf{k}}^\dagger)$, $a_{j,\mathbf{k}}^\dagger (j = 1, 2, \dots, M)$ is a spin-wave (boson) creation operator, and M represents the internal degrees of freedom within a unit cell. The Bloch Hamiltonian $\mathcal{H}(\mathbf{k})$ is a $2M \times 2M$ Hermitian matrix, and is generally expressed as

$$\mathcal{H}(\mathbf{k}) = \begin{pmatrix} \mathcal{A}_{\mathbf{k}} & \mathcal{B}_{\mathbf{k}} \\ \mathcal{B}_{-\mathbf{k}}^* & \mathcal{A}_{-\mathbf{k}}^* \end{pmatrix}, \quad (\text{A2})$$

with $M \times M$ matrices $\mathcal{A}_{\mathbf{k}}$ and $\mathcal{A}_{-\mathbf{k}}^*$ for the normal channel, and $M \times M$ matrices $\mathcal{B}_{\mathbf{k}}$ and $\mathcal{B}_{-\mathbf{k}}^*$ for the anomalous channel. To diagonalize such a bosonic BdG Hamiltonian, we should introduce a paraunitary matrix $\mathcal{T}(\mathbf{k})$ instead of a unitary matrix [31],

$$\mathcal{T}^\dagger(\mathbf{k}) \mathcal{H}(\mathbf{k}) \mathcal{T}(\mathbf{k}) = \begin{pmatrix} E_{\mathbf{k}} & \\ & E_{-\mathbf{k}} \end{pmatrix}, \quad (\text{A3})$$

where $E_{\mathbf{k}}$ is a $M \times M$ diagonal matrix with its diagonal elements representing the magnon energy eigenvalues. The paraunitary matrix $\mathcal{T}(\mathbf{k})$ changes the old basis $(\beta_{\mathbf{k}}^\dagger, \beta_{-\mathbf{k}})$ into a new basis $(\gamma_{\mathbf{k}}^\dagger, \gamma_{-\mathbf{k}})$ as

$$(\gamma_{\mathbf{k}}^\dagger, \gamma_{-\mathbf{k}}) \mathcal{T}^\dagger(\mathbf{k}) = (\beta_{\mathbf{k}}^\dagger, \beta_{-\mathbf{k}}), \quad (\text{A4})$$

and it satisfies

$$\mathcal{T}^\dagger(\mathbf{k})\Sigma_3\mathcal{T}(\mathbf{k}) = \Sigma_3, \quad \mathcal{T}(\mathbf{k})\Sigma_3\mathcal{T}^\dagger(\mathbf{k}) = \Sigma_3, \quad (\text{A5})$$

with a diagonal $2M \times 2M$ diagonal matrix $\Sigma_3 = s_z \otimes I_{M \times M}$, where s_z is the z component of the 2×2 Pauli matrices, and $I_{M \times M}$ is a $M \times M$ identity matrix. The Hermitian BdG Hamiltonian $\mathcal{H}(\mathbf{k})$ should be a positive-definite matrix in order to ensure that the magnon excitation energies are positive for any \mathbf{k} .

The paraunitary matrix $\mathcal{T}(\mathbf{k})$ used to diagonalize $\mathcal{H}(\mathbf{k})$ can be obtained by the following procedure. First, we decompose $\mathcal{H}(\mathbf{k})$ into a product between an upper triangle matrix $\mathcal{K}(\mathbf{k})$ and its Hermitian conjugate, $\mathcal{H}(\mathbf{k}) = \mathcal{K}^\dagger(\mathbf{k})\mathcal{K}(\mathbf{k})$ by the Cholesky decomposition. The Cholesky decomposition is possible as long as the BdG Hamiltonian $\mathcal{H}(\mathbf{k})$ is positive definite. Then we diagonalize a matrix $\mathcal{W}(\mathbf{k}) \equiv \mathcal{K}(\mathbf{k})\Sigma_3\mathcal{K}^\dagger(\mathbf{k})$ as

$$\mathcal{U}(\mathbf{k})^\dagger\mathcal{W}(\mathbf{k})\mathcal{U}(\mathbf{k}) = \begin{pmatrix} E_{\mathbf{k}} & \\ & -E_{-\mathbf{k}} \end{pmatrix}, \quad (\text{A6})$$

by introducing a unitary matrix $\mathcal{U}(\mathbf{k})$. Here, $E_{\mathbf{k}}$ is an $M \times M$ diagonal matrix with positive diagonal elements. Finally, the paraunitary matrix is obtained as

$$\mathcal{T}(\mathbf{k}) = \mathcal{K}^{-1}(\mathbf{k})\mathcal{U}(\mathbf{k}) \begin{pmatrix} E_{\mathbf{k}}^{1/2} & \\ & E_{-\mathbf{k}}^{1/2} \end{pmatrix}, \quad (\text{A7})$$

which satisfies Eq. (A5). Thus, by means of the Cholesky decomposition, we can obtain the magnon bands from the bosonic BdG Hamiltonian.

Appendix B: Geometric term of in bosonic BdG formalization

In this appendix, we explain how to calculate the geometric term of the number of magnons \hat{N} for the bosonic BdG formalization mentioned in the main text. In Appendix A, we showed that a generic BdG bosonic Hamiltonian Eq. (A1) is written as the quadratic form in the basis $(\beta_{\mathbf{k}}^\dagger, \beta_{-\mathbf{k}})$, and meanwhile the matrix of the number of magnons \hat{N} in the same basis is an identity matrix

which is expressed as

$$\hat{N} = \frac{1}{2} \sum_{\mathbf{k}} (\beta_{\mathbf{k}}^\dagger, \beta_{-\mathbf{k}}) \begin{pmatrix} \beta_{\mathbf{k}} \\ \beta_{-\mathbf{k}}^\dagger \end{pmatrix}. \quad (\text{B1})$$

The BdG Bloch Hamiltonian can be diagonalized by the basis transformation of Eq. (A4) to $(\gamma_{\mathbf{k}}^\dagger, \gamma_{-\mathbf{k}})$, and the time-dependent matrix of the BdG Bloch Hamiltonian can be written as

$$\begin{aligned} \hat{H}(\tau) &= \frac{1}{2} \sum_{\mathbf{k}} (\beta_{\mathbf{k}}^\dagger(\tau), \beta_{-\mathbf{k}}(\tau)) \mathcal{H}(\mathbf{k}, \tau) \begin{pmatrix} \beta_{\mathbf{k}}(\tau) \\ \beta_{-\mathbf{k}}^\dagger(\tau) \end{pmatrix} \\ &= \frac{1}{2} \sum_{\mathbf{k}} (\gamma_{\mathbf{k}}^\dagger, \gamma_{-\mathbf{k}}) \begin{pmatrix} E_{\mathbf{k}}(\tau) & \\ & E_{-\mathbf{k}}(\tau) \end{pmatrix} \begin{pmatrix} \gamma_{\mathbf{k}} \\ \gamma_{-\mathbf{k}}^\dagger \end{pmatrix}, \end{aligned} \quad (\text{B2})$$

which becomes diagonal and the time dependence is reduced into the diagonal matrix. Here $E_{\mathbf{k}}$ is a $M \times M$ matrix whose diagonal elements show the particle dispersion of bosons. Meanwhile, the number of magnon becomes

$$\hat{N}(\tau) = \frac{1}{2} \sum_{\mathbf{k}} (\gamma_{\mathbf{k}}^\dagger, \gamma_{-\mathbf{k}}) \mathcal{T}^\dagger(\mathbf{k}, \tau) \mathcal{T}(\mathbf{k}, \tau) \begin{pmatrix} \gamma_{\mathbf{k}} \\ \gamma_{-\mathbf{k}}^\dagger \end{pmatrix}. \quad (\text{B3})$$

Therefore, in Eq. (21), the matrix elements of the number operator of magnons (Eq. (22)) and those of the Berry connection (Eq. (23)) are rewritten as

$$\hat{N}_{nm}(\mathbf{k}, \tau) = \frac{1}{2} \left\{ \mathcal{T}^\dagger(\mathbf{k}, \tau) \mathcal{T}(\mathbf{k}, \tau) \right\}_{nm}, \quad (\text{B4})$$

and

$$A_{mn}(\mathbf{k}, \tau) = -i \frac{\left\{ \mathcal{T}^\dagger(\mathbf{k}, \tau) \partial_\tau \mathcal{H}(\mathbf{k}, \tau) \mathcal{T}(\mathbf{k}, \tau) \right\}_{mn}}{E_{n,\mathbf{k}}(\tau) - E_{m,\mathbf{k}}(\tau)}, \quad (\text{B5})$$

respectively.

-
- [1] A. Einstein and W. J. de Hass, Verh. Dtsch. Phys. Ges. **17**, 152 (1915).
[2] S. J. Barnett, Phys. Rev. **6**, 239 (1915).
[3] M. Matsuo, J. Ieda, K. Harii, E. Saitoh, and S. Maekawa, Phys. Rev. B **87**, 180402(R) (2013).
[4] M. Matsuo, J. Ieda, E. Saitoh, and S. Maekawa, Phys. Rev. Lett. **106**, 076601 (2011).
[5] M. Matsuo, J. Ieda, E. Saitoh, and S. Maekawa, Phys. Rev. B **84**, 104410 (2011).
[6] L. Zhang and Q. Niu, Phys. Rev. Lett. **112**, 085503

- (2014).
[7] L. Zhang and Q. Niu, Phys. Rev. Lett. **115**, 115502 (2015).
[8] T. Zhang and S. Murakami, Phys. Rev. Research **4**, L012024 (2022).
[9] H. Chen, W. Wu, S. A. Yang, X. Li, and L. Zhang, Phys. Rev. B **100**, 094303 (2019).
[10] H. Komiyama and S. Murakami, Phys. Rev. B **103**, 214302 (2021).
[11] Q. Wang, S. Li, J. Zhu, H. Chen, W. Wu, W. Gao, L.

- Zhang, and S. A. Yang, Phys. Rev. B. **105**, 104301 (2022).
- [12] J. Fransson, Phys. Rev. Research **5**, L022039 (2023).
- [13] H. Zhu, J. Yi, M.-Y. Li, J. Xiao, L. Zhang, C.-W. Yang, R. A. Kaindl, L.-J. Li, Y. Wang, and X. Zhang, Science **359**, 579 (2018).
- [14] K. Ishito, H. Mao, Y. Kousaka, Y. Togawa, S. Iwasaki, T. Zhang, S. Murakami, J. Kishine, and T. Satoh, Nature Phys. (2022).
- [15] M. V. Berry, Proc. R. Soc. Lond. A, **392**, 45 (1985).
- [16] L. Trifunovic, S. Ono, and H. Watanabe, Phys. Rev. B **100**, 054408 (2019).
- [17] M. Hamada and S. Murakami, Phys. Rev. Research **2**, 023275 (2020).
- [18] D. Yao and S. Murakami, Phys. Rev. B **105**, 184412 (2022).
- [19] R. Shindou, R. Matsumoto, S. Murakami, and J.I. Ohe, Phys. Rev. B **87**, 174427 (2013).
- [20] R. Shindou, J.I. Ohe, R. Matsumoto, S. Murakami, and E. Saitoh, Phys. Rev. B **87**, 174402 (2013).
- [21] R. Matsumoto and S. Murakami, Phys. Rev. Lett. **106**, 197202 (2011).
- [22] R. Matsumoto and S. Murakami, Phys. Rev. B **84**, 184406 (2011).
- [23] R. Matsumoto, R. Shindou, and S. Murakami, Phys. Rev. B **89**, 054420 (2014).
- [24] X. Zhai and Y. M. Blanter, Phys. Rev. B **102**, 075407 (2020).
- [25] T. Ideue, Y. Onose, H. Katsura, Y. Shiomi, S. Ishiwata, N. Nagaosa, and Y. Tokura, Phys. Rev. B **85**, 134411 (2012).
- [26] Y. Onose, T. Ideue, H. Katsura, Y. Shiomi, N. Nagaosa, and Y. Tokura, Science **329**, 297 (2010).
- [27] A. Mook, J. Henk, and I. Mertig, Phys. Rev. B **89**, 134409 (2014).
- [28] T. Moriya, Phys. Rev. **120**, 1 (1960).
- [29] C. Berk, M. Jars, W. Yang, S. Dhuey, S. Cabrini, and H. Schmidt, Nature Comm. **10**, 2652 (2019).
- [30] J. Fransson, Nano Lett. **21**, 3026 (2021).
- [31] H. H. P. Colpa, Physica A **93**, 327 (1978).